Investigation of fully heavy tetraquark within chiral quark model*

Yuheng Wu (吴雨衡)[1] Xuejie Liu (刘雪杰)[2] Ye Yan (颜晔)[3] Yue Tan (谭悦)[1] Qi Huang (黄琦)[4†]
Hongxia Huang (黄虹霞)[4‡] Jialun Ping (平加伦)[4]

[1]Department of Physics, Yancheng Institute of Technology, Yancheng 224000, China
[2]Department of Physics, Henan Normal University, Xinxiang 453007, China
[3]Department of Physics, Changzhou College of Information Technology, Changzhou 213164, China
[4]Department of Physics, Nanjing Normal University, Nanjing 210097, China

Abstract: In the framework of the Chiral quark model (ChQM), we investigate fully charmed and fully bottom tetraquarks with $J^{PC}=2^{++}$ by considering two structures: $Q\bar{Q}-Q\bar{Q}$ and $QQ-\bar{Q}\bar{Q}$. The bound-state calculation shows that there are no bound states in either the $cc\bar{c}\bar{c}$ or $bb\bar{b}\bar{b}$ systems. However, using the real-scaling method, we obtain several resonant states. For the $cc\bar{c}\bar{c}$ system, when the channel coupling includes only three S-wave channels, two resonant states are obtained: one with a mass of approximately 7002 MeV and a decay width of about 54 MeV, and another with a mass of approximately 7227 MeV and a decay width of about 66 MeV. The former can be regarded as a candidate for the $X(6900)$, whereas the latter can be considered a candidate for the $X(7200)$. After adding the $\chi_{c0}\chi_{c2}$, $\chi_{c1}\chi_{c1}$, $\chi_{c1}\chi_{c2}$, and $\chi_{c2}\chi_{c2}$ channels, both resonant states remain. For the $bb\bar{b}\bar{b}$ system, only one resonant state is obtained, regardless of whether the four excited-meson channels are included. The mass and width of this resonant state are approximately 19743 MeV and 67 MeV, respectively. We suggest that future experiments search for this possible resonant state in the invariant mass spectrum of $\Upsilon\Upsilon$ or $\Upsilon\Upsilon(2S)$.

Keywords: quark model, tetraquark state, resonance state

DOI: 10.1088/1674-1137/ae9c1d **CSTR:** 32044.14.ChinesePhysicsC.50113110

I. INTRODUCTION

Following the initial observation of the $X(3872)$ by the Belle Collaboration in 2003 [1], experiments have identified a growing number of analogous exotic (XYZ) states. The exploration of exotic states beyond the conventional quark model has emerged as a frontier in particle physics, challenging our understanding of quantum chromodynamics (QCD) and the fundamental nature of strong interactions.

Fully heavy tetraquark states provide a relatively clean platform for studying strong interactions, as they are not affected by long-range light-meson exchange mechanisms. Experimentally, the exploration of fully heavy tetraquark states can be traced back to the production of Y pairs reported by the CMS Collaboration in 2017 [2]. In 2019, the ANDY Collaboration reported a significant structure around 18.2 GeV in Cu+Au collisions [3]. However, in 2020, the LHCb Collaboration found no significant signal in the $\Upsilon(1S)\mu^+\mu^-$ invariant mass spectrum at centre-of-mass energies $\sqrt{s}=7,8$ and 13 TeV [4]. Moreover, the updated analysis by the CMS Collaboration also revealed no significant excess of events compatible with a narrow resonance [5]. From a theoretical perspective, several studies have explored the possible existence of fully bottomed tetraquark states [6−10]. However, the existence of fully bottomed tetraquark states remains to be conclusively established through rigorous experimental investigation.

The progress in the experimental exploration of fully charmed tetraquark states has been particularly encouraging. In 2020, the LHCb Collaboration discovered a new resonant state, $X(6900)$, with a global significance exceeding 5σ in the $J/\psi J/\psi$ invariant mass spectrum, along with a broad enhancement spanning 6.2–6.8 GeV and a

Received 10 June 2026; Accepted 20 August 2026; Accepted manuscript online 21 August 2026

* This work is partly supported by the National Natural Science Foundation of China (12575088, 11675080, 11775118, 11535005, 12305087); the Funding for School-Level Research Projects of Yancheng Institute of Technology (xjr2025010, 2022039); the Start-up Funds of Nanjing Normal University (184080H201B20); the School-Level Research Projects of Henan Normal University (20240304), and the Changzhou Sci&Tech Program (20260098). Yue Tan is supported by the Qinglan Project of Jiangsu Province of China

† E-mail: 06289@njnu.edu.cn
‡ E-mail: hxhuang@njnu.edu.cn

Content from this work may be used under the terms of the Creative Commons Attribution 3.0 licence. Any further distribution of this work must maintain attribution to the author(s) and the title of the work, journal citation and DOI. Article funded by SCOAP[3] and published under licence by Chinese Physical Society and the Institute of High Energy Physics of the Chinese Academy of Sciences and the Institute of Modern Physics of the Chinese Academy of Sciences and IOP Publishing Ltd

preliminary indication of an additional structure around 7.2 GeV [11]. Subsequently, the CMS [12] and ATLAS [13] Collaborations independently confirmed the existence of the $X(6900)$ state. Furthermore, the CMS Collaboration reported two additional states, denoted as $X(6600)$ and $X(7200)$, in the di-J/ψ invariant mass spectrum with and without interference effects. In the di-J/ψ decay channel, the ATLAS Collaboration not only confirmed the $X(6900)$ but also identified two new structures, $X(6400)$ and $X(6600)$. Meanwhile, in the $J/\psi\psi(2S)$ decay channel, signals of the $X(6900)$ and a new $X(7200)$ state were observed.

Prior to the experimental observation of the $X(6900)$ by the LHCb Collaboration, fully heavy tetraquark states had been extensively investigated in the literature [14−32]. Following the experimental discovery of the exotic states mentioned above, a wide range of theoretical methods have been applied, including the constituent quark model [33−46], QCD sum rules [47−59], potential models [60−63], the Bethe-Sapeter framework [64, 65] and other approaches [66−83]. The authors of Ref. [35] used two constituent quark models, namely the quark delocalization color screening model and the chiral quark model, to study fully heavy tetraquark states. Their computational results show that, for fully bottomed systems, the chiral quark model yields no bound or resonance states in either of the two structures considered, namely the meson-meson and diquark-antidiquark structures. However, the quark delocalization color screening model suggests the possible existence of broad resonances with masses ranging from 19.1 to 19.4 GeV and quantum numbers $J^P = 0^+$, 1^+, and 2^+. For fully charmed tetraquark states, the $X(6900)$ can be interpreted as a compact resonance state with $IJ^P = 00^+$. Zhang *et al.* [37] employed a nonrelativistic constituent quark model to study the S-wave fully heavy tetraquark states. They showed that the $X(6900)$ may not be a ground $cc\bar{c}\bar{c}$ tetraquark state, whereas the $X(6600)$ can be interpreted as a ground fully charmed tetraquark state with spin-parity $J^{PC} = 0^{++}$. Moreover, states with $bb\bar{b}\bar{b}$ components could be located around 19.2 GeV. In Ref. [38], the authors identified promising candidates for the $X(6900)$ and $X(7200)$ in both the $J^{PC} = 0^{++}$ and 2^{++} systems. In addition, for the fully bottomed tetraquark system, they predicted several resonant states in the 19.7−20.0 GeV mass range. Studies on the decays and production of fully heavy tetraquarks can also be found in Refs. [84−103].

In our previous work [104], we studied the $cc\bar{c}\bar{c}$ system with $J^{PC} = 0^{++}$, because this quantum number includes more channels and thus contains richer physical information. Four resonance states with energies around 6923, 6996, 7060 and 7159 MeV were obtained. However, the decay width of the resonance state at 6923 MeV is only 10.1 MeV, which is much smaller than the experimental measurement. Recently, the CMS Collaboration proposed that the quantum numbers of fully charmed tetraquark states tend to be $J^{PC} = 2^{++}$ [105]. Given that the experimental data tend to favor the $J^{PC} = 2^{++}$ assignment, in this work we systematically investigate the $cc\bar{c}\bar{c}$ states with $J^{PC} = 2^{++}$ to search for candidates for the experimentally reported states within the framework of the chiral quark model. Moreover, we extend our study to the $bb\bar{b}\bar{b}$ system with the same quantum number.

The structure of this paper is as follows. Section II provides a brief description of the quark model and wave functions. Section III presents the numerical results and discussion. The summary is given in the final section.

II. MODEL AND WAVE FUNCTIONS

A. Chiral quark model (ChQM)

In this work, we use the chiral quark model (ChQM) to investigate the $QQ\bar{Q}\bar{Q}$ $(Q = c, b)$ tetraquark system. Details of the ChQM can be found in Refs. [20, 106]. Here, we present only the Hamiltonian of the model

$$H = \sum_{i=1}^{4}\left(m_i + \frac{p_i^2}{2m_i}\right) - T_{\rm CM} + \sum_{j>i=1}^{4}(V_{\rm CON} + V_{\rm OGE}). \tag{1}$$

Because the quark composition of the system under study consists entirely of heavy quarks, the Goldstone-boson and σ-meson exchange terms are absent; therefore, these two terms are omitted from Eq. (1). m_i $(i = c/b)$ denotes the constituent mass of the charm or bottom quark. $T_{\rm CM}$ is the kinetic energy of the center of mass.

$V_{\rm CON}$ is the confinement interaction, which includes central ($V_{\rm CON}^{\rm C}$) and spin-orbit ($V_{\rm CON}^{\rm SO}$) components, and can be written as follows:

$$V_{\rm CON}^{\rm C} = (-a_c r_{ij}^2 - \Delta)\boldsymbol{\lambda}_i^c \cdot \boldsymbol{\lambda}_j^c, \tag{2a}$$

$$\begin{aligned} V_{\rm CON}^{\rm SO} = & -\boldsymbol{\lambda}_i^c \cdot \boldsymbol{\lambda}_j^c \frac{a_c}{4m_i^2 m_j^2}[((m_i^2 + m_j^2)(1 - 2a_s) \\ & + 4m_i m_j(1 - a_s))(\vec{S}_+ \cdot \vec{L}) \\ & + ((m_j^2 - m_i^2)(1 - 2a_s))(\vec{S}_- \cdot \vec{L})], \end{aligned} \tag{2b}$$

where a_c is the confinement strength, Δ is a global constant that fixes the energy origin, and a_s determines the ratio between the scalar and vector terms.

$V_{\rm OGE}$ is the one-gluon-exchange interaction, which includes central ($V_{\rm OGE}^{\rm C}$), spin-orbit ($V_{\rm OGE}^{\rm SO}$), and tensor ($V_{\rm OGE}^{\rm T}$) forces and can be expressed as follows:

$$V_{\rm OGE}^{\rm C} = \frac{\alpha_s}{4}\boldsymbol{\lambda}_i^c \cdot \boldsymbol{\lambda}_j^c \left[\frac{1}{r_{ij}} - \frac{1}{6m_i m_j r_0^2}\boldsymbol{\sigma}_i \cdot \boldsymbol{\sigma}_j \frac{{\rm e}^{-\frac{r_{ij}}{r_0}}}{r_{ij}}\right], \tag{3a}$$

$$V_{\rm OGE}^{\rm SO} = -\frac{1}{16}\frac{\alpha_s \boldsymbol{\lambda}_i^c \cdot \boldsymbol{\lambda}_j^c}{4m_i^2 m_j^2}\left[\frac{1}{r_{ij}^3} - \frac{{\rm e}^{-r_{ij}/r_g(\mu)}}{r_{ij}^3}\left(1+\frac{r_{ij}}{r_g(\mu)}\right)\right] [(m_i^2+m_j^2+4m_i m_j)(\vec{S}_+\cdot\vec{L}) + (m_j^2-m_i^2)(\vec{S}_-\cdot\vec{L})], \tag{3b}$$

$$V_{\rm OGE}^{\rm T} = -\frac{1}{16}\frac{\alpha_s \boldsymbol{\lambda}_i^c \cdot \boldsymbol{\lambda}_j^c}{4m_i^2 m_j^2}\left[\frac{1}{r_{ij}^3} - \frac{{\rm e}^{-r_{ij}/r_g(\mu)}}{r_{ij}}\left(\frac{1}{r_{ij}^2} + \frac{1}{3r_g^2(\mu)} + \frac{1}{r_{ij}r_g(\mu)}\right)\right] S_{ij}, \tag{3c}$$

where $\boldsymbol{\sigma}$ represents the $SU(2)$ Pauli matrices; α_s denotes the quark–gluon coupling constant (in Table 1, $\alpha_{s_{cc}}$ and $\alpha_{s_{bb}}$ denote the quark–gluon coupling constants for $c\bar{c}$ and $b\bar{b}$ quark interactions, respectively); $r_0 = \hat{r}_0/\mu$, which scales with the reduced mass as expected for a Coulombic system; and $r_g(\mu) = \hat{r}_g/\mu$, which exhibits scaling behavior similar to that of the central term.

Table 1. Quark model parameters.

m_c/MeV	m_b/MeV	a_c/MeV	Δ/MeV	$\hat{r}_0$/MeV	$\hat{r}_g$/MeV
1650	4977	98	–18.1	81.0	100.6
$\alpha_{s_{cc}}$	$\alpha_{s_{bb}}$	a_s			
0.56	0.43	0.77			

Table 2. Numerical results from the present work (with a harmonic confinement form) and ChQM2 (with a color-screening confinement form) (unit: MeV).

Meson	This work	ChQM2 [106]	EXP.(PDG) [107]
η_c	2980	2990	2983.9
$\eta_c(2S)$	3637	3627	3637.7
$\eta_c(3S)$	4132	–	–
J/ψ	3100	3097	3096.9
$\psi(2S)$	3713	3685	3686.1
χ_{c0}	3420	3436	3414.7
χ_{c1}	3479	3494	3510.6
χ_{c2}	3523	3526	3556.1
η_b	9390	9454	9398.7
Υ	9502	9505	9460.3
$\Upsilon(2S)$	9971	10013	10023.2
$\Upsilon(3S)$	10289	10335	10355.2
χ_{b0}	9865	9855	9859.4
χ_{b1}	9891	9875	9892.7
χ_{b2}	9908	9887	9912.2

The other symbols in the above expressions have their usual meanings. In this work, all parameters listed in Table 1 are determined by fitting the calculated meson spectrum to the experimental data. The meson masses calculated in the present work are shown in Table 2.

B. Wave function

For the fully heavy system, meson-meson and diquark-antidiquark structures (denoted hereafter as $Q\bar{Q}$-$Q\bar{Q}$ and QQ-$\bar{Q}\bar{Q}$, respectively) are considered. The wave function of each structure consists of four components: orbital, flavor, spin, and color wave functions. Considering the spin-orbit coupling effect, the spin and orbital wave functions must be coupled, whereas the flavor and color wave functions are independent.

In the Gaussian expansion method (GEM), the radial part of the spatial wave function is expanded in terms of Gaussian functions [108]:

$$\Psi_L(\mathbf{r}) = \sum_{n=1}^{n_{\max}} c_n \psi_{nlm}^G(\mathbf{r}), \tag{4a}$$

$$\psi_{nlm}^G(\mathbf{r}) = N_{nl} r^l {\rm e}^{-\nu_n r^2} Y_{lm}(\hat{\mathbf{r}}), \tag{4b}$$

where the N_{nl} are normalization constants

$$N_{nl} = \left[\frac{2^{l+2}(2\nu_n)^{l+\frac{3}{2}}}{\sqrt{\pi}(2l+1)}\right]^{\frac{1}{2}}. \tag{5}$$

The coefficients c_n are variational parameters that are determined dynamically. The Gaussian size parameters are chosen according to the following geometric progression:

$$\nu_n = \frac{1}{r_n^2}, \quad r_n = r_1 a^{n-1}, \quad a = \left(\frac{r_{n_{\max}}}{r_1}\right)^{\frac{1}{n_{\max}-1}}. \tag{6}$$

This procedure enables optimization of the ranges using only a small number of Gaussians.

For the spin wave functions, no distinction is made between quarks and antiquarks. The meson-meson structure has the same spin as the diquark-antidiquark structure. The spin wave functions of the subclusters are given as follows:

$$\chi_{11}^\sigma = \alpha\alpha,\ \chi_{10}^\sigma = \frac{1}{\sqrt{2}}(\alpha\beta+\beta\alpha), \quad \chi_{1-1}^\sigma = \beta\beta,\ \chi_{00}^\sigma = \frac{1}{\sqrt{2}}(\alpha\beta-\beta\alpha). \tag{7}$$

Once the orbital and spin wave functions have been ob-

tained, the next step is to couple these two types of wave functions. First, $|\psi_{J_1},m_{J_1}\rangle$ is obtained by coupling the orbital wave function $|\psi_{L_1},m_{L_1}\rangle$ and the spin wave function $|\chi^{\sigma}_{S_1},m_{S_1}\rangle$ of the first subcluster

$$|\psi_{J_1,m_{J_1}}\rangle = |\psi_{L_1,m_{L_1}}\rangle \otimes |\chi^{\sigma}_{S_1,m_{S_1}}\rangle. \tag{8}$$

Similarly, the orbital wave function $|\psi_{L_2},m_{L_2}\rangle$ and spin wave function $|\chi^{\sigma}_{S_2},m_{S_2}\rangle$ of the second subcluster are combined to form $|\psi_{J_2},m_{J_2}\rangle$:

$$|\psi_{J_2,m_{J_2}}\rangle = |\psi_{L_2,m_{L_2}}\rangle \otimes |\chi^{\sigma}_{S_2,m_{S_2}}\rangle. \tag{9}$$

Subsequently, the wave functions of the two subclusters are coupled to form $|\psi_{J_{12}},m_{J_{12}}\rangle$:

$$|\psi_{J_{12},m_{J_{12}}}\rangle = |\psi_{J_1,m_{J_1}}\rangle \otimes |\psi_{J_2,m_{J_2}}\rangle. \tag{10}$$

In the final step, the wave function $|\psi_{J_{12}},m_{J_{12}}\rangle$ is coupled to the orbital wave function $|\psi_{L_3},m_{L_3}\rangle$ describing the relative motion between the two subclusters, generating the total orbit-spin wave function $|\psi^{LS}_i\rangle$:

$$|\psi^{LS}_i\rangle = |\psi_{J_{12},m_{J_{12}}}\rangle \otimes |\psi_{L_3,m_{L_3}}\rangle, \tag{11}$$

$$i \equiv [J_1, J_2, J_{12}, L_3]. \tag{12}$$

In this work, we focus on the 2^{++} system and consider a total of 5 combinations for $[J_1, J_2, J_{12}, L_3]$, with the intercluster relative motion fixed in the S wave ($L_3 = 0$), as shown in Table 3.

For the flavor wave function, different structures are obtained depending on the coupling sequence. For the $Q\bar{Q}$-$Q\bar{Q}$ structure, the coupling sequence is

$$|F_1\rangle = Q_1\bar{Q}_2Q_3\bar{Q}_4. \tag{13}$$

Table 3. Different combinations of J–J coupling.

$L_3=0$	$J_1=0$		$J_2=2$		index(i)
	$L_1=1$	$S_1=1$	$L_2=1$	$S_2=1$	1
	$J_1=1$		$J_2=1$		index(i)
	$L_1=0$	$S_1=1$	$L_2=0$	$S_2=1$	2
	$L_1=1$	$S_1=1$	$L_2=1$	$S_2=1$	3
	$J_1=1$		$J_2=2$		index(i)
	$L_1=1$	$S_1=1$	$L_2=1$	$S_2=1$	4
	$J_1=2$		$J_2=2$		index(i)
	$L_1=1$	$S_1=1$	$L_2=1$	$S_2=1$	5

For the QQ-$\bar{Q}\bar{Q}$ structure, the coupling sequence is

$$|F_2\rangle = Q_1Q_3\bar{Q}_2\bar{Q}_4. \tag{14}$$

The colorless tetraquark system has four color structures: $1\otimes1$, $8\otimes8$, $\bar{3}\otimes3$, and $6\otimes\bar{6}$:

$$\begin{aligned}
|C_1\rangle &= \chi^{m1}_{1\otimes1} = \frac{1}{\sqrt{9}}(\bar{r}r\bar{r}r + \bar{r}r\bar{g}g + \bar{r}r\bar{b}b + \bar{g}g\bar{r}r + \bar{g}g\bar{g}g \\
&\quad + \bar{g}g\bar{b}b + \bar{b}b\bar{r}r + \bar{b}b\bar{g}g + \bar{b}b\bar{b}b), \\
|C_2\rangle &= \chi^{m2}_{8\otimes8} = \frac{\sqrt{2}}{12}(3\bar{b}r\bar{r}b + 3\bar{g}r\bar{r}g + 3\bar{b}g\bar{g}b + 3\bar{g}b\bar{b}g \\
&\quad + 3\bar{r}g\bar{g}r + 3\bar{r}b\bar{b}r + 2\bar{r}r\bar{r}r + 2\bar{g}g\bar{g}g + 2\bar{b}b\bar{b}b - \bar{r}r\bar{g}g \\
&\quad - \bar{g}g\bar{r}r - \bar{b}b\bar{g}g - \bar{b}b\bar{r}r - \bar{g}g\bar{b}b - \bar{r}r\bar{b}b), \\
|C_3\rangle &= \chi^{d1}_{\bar{3}\otimes3} = \frac{\sqrt{3}}{6}(rg\bar{r}\bar{g} - rg\bar{g}\bar{r} + gr\bar{g}\bar{r} - gr\bar{r}\bar{g} + rb\bar{r}\bar{b}, \\
&\quad - rb\bar{b}\bar{r} + br\bar{b}\bar{r} - br\bar{r}\bar{b} + gb\bar{g}\bar{b} - gb\bar{b}\bar{g} + bg\bar{b}\bar{g} - bg\bar{g}\bar{b}), \\
|C_4\rangle &= \chi^{d2}_{6\otimes\bar{6}} = \frac{\sqrt{6}}{12}(2rr\bar{r}\bar{r} + 2gg\bar{g}\bar{g} + 2bb\bar{b}\bar{b} + rg\bar{r}\bar{g} \\
&\quad + rg\bar{g}\bar{r} + gr\bar{g}\bar{r} + gr\bar{r}\bar{g} + rb\bar{r}\bar{b} + rb\bar{b}\bar{r} + br\bar{b}\bar{r} \\
&\quad + br\bar{r}\bar{b} + gb\bar{g}\bar{b} + gb\bar{b}\bar{g} + bg\bar{b}\bar{g} + bg\bar{g}\bar{b}).
\end{aligned} \tag{15}$$

Here, $|C_1\rangle$, $|C_2\rangle$, $|C_3\rangle$ and $|C_4\rangle$ represent the color singlet-singlet ($1\otimes1$), color octet-octet ($8\otimes8$), color triplet-antitriplet ($\bar{3}\otimes3$), and color sextet-antisextet ($6\otimes\bar{6}$) wave functions, respectively. The state with the color wave function $|C_1\rangle$ corresponds to the color-singlet channel, whereas those with $|C_2\rangle$, $|C_3\rangle$, or $|C_4\rangle$ correspond to hidden-color channels.

Finally, the total wave function of the tetraquark system is written as:

$$\Psi^{i,j,k}_{JM_J} = \mathcal{A}\psi^{LS}_i F_j C_k, \tag{16}$$

Here, $\mathcal{A}$ is the antisymmetrization operator. For the $QQ\bar{Q}\bar{Q}$ system, $\mathcal{A} = 1 - P_{13} - P_{24} + P_{13,24}$. We then solve the following Schrödinger equation to obtain the eigenenergies of the system using the Rayleigh-Ritz variational principle

$$H\Psi^{i,j,k}_{JM_J} = E\Psi^{i,j,k}_{JM_J}, \tag{17}$$

where $\Psi^{i,j,k}_{JM_J}$ is the wave function of the four-quark states, expressed as a linear combination of the channel wave functions defined above.

III. REAL-SCALING METHOD

The real-scaling method, also known as the stabilization method [109], was developed to distinguish genuine resonances from states with discrete energies in finite-volume calculations. This method has been successfully applied to tetraquark systems [110] and pentaquark systems [111, 112]. In this method, a factor α is used to scale the finite volume. As α increases, false resonances decay into the corresponding threshold channels, whereas genuine resonances appear as avoided-crossing configurations (as shown in Fig. 1). The avoided-crossing structure arises because the energy of one scattering state approaches that of the resonance state as the scaling factor increases and the coupling becomes stronger. This structure is a general property of interacting two-level systems. The details have been discussed in Refs. [104, 114, 115].

To calculate the decay widths of the resonance states, we employ the formula from Ref. [109]:

$$\Gamma = 4|V(\alpha_c)|\frac{\sqrt{|S_r||S_c|}}{|S_r - S_c|}, \tag{18}$$

where $V(\alpha_c)$ represents the minimal energy difference between the resonance state and the scattering state; S_r and S_c are the slopes of the resonance and scattering states, respectively (see Fig. 1).

IV. RESULT AND DISCUSSION

In this work, we investigate fully charmed and fully bottomed tetraquark systems with the quantum number $J^{PC} = 2^{++}$ within the ChQM framework. Two structures, $Q\bar{Q}$-$Q\bar{Q}$ and QQ-$\bar{Q}\bar{Q}$, as well as the channel coupling between these two configurations, are considered. In addition to calculating bound states, we employ the real-scaling method to search for possible resonant states in the system. We also conduct a comparative study of the effects of including and excluding channels composed of excited mesons (χ_{Q0}, χ_{Q1}, χ_{Q2}, $Q = c$ or b) on the results. The notation $\chi_{Q0,1,2}$ ($Q = c, b$) denotes P-wave charmonium/bottomonium states, where the subscripts $0, 1, 2$ indicate the total angular momentum of the $Q\bar{Q}$ ($Q = c, b$) state.

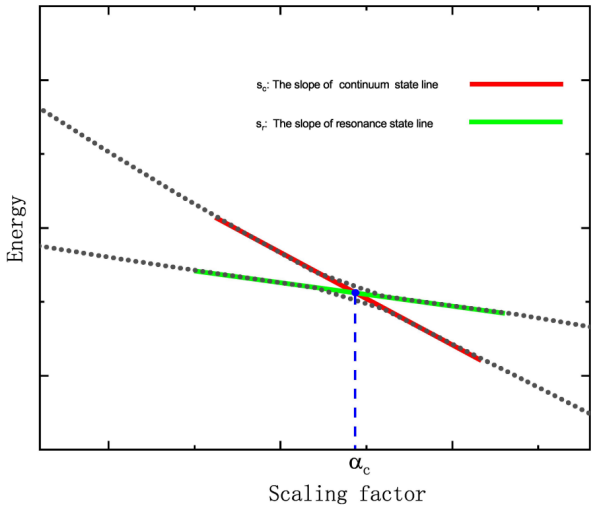


Fig. 1. (color online) A schematic energy spectrum obtained using the real-scaling method [113].

A. Fully charmed tetraquark system

The energies of the $cc\bar{c}\bar{c}$ tetraquark system for the $c\bar{c}$-$c\bar{c}$ and cc-$\bar{c}\bar{c}$ structures, as well as the channel coupling of these two structures, are listed in Table 4. Here, $E_{\rm th}$ represents the theoretical threshold; $E_{\rm sc}$ is the energy of each single channel; $E_{\rm mix1}$ is the lowest energy of the system obtained by coupling three S-wave channels ($J/\psi J/\psi$, $[J/\psi]_8[J/\psi]_8$, $[cc]^1_{\bar{3}}[\bar{c}\bar{c}]^1_3$); and $E_{\rm mix2}$ denotes the lowest energy of the system obtained by coupling all seven channels of both configurations.

For the $J^{PC} = 2^{++}$ system, we analyze seven channels, including five color-singlet channels and two color-exotic channels (an octet-octet channel and a triplet-anti-triplet channel). As shown in Table 4, the energies of the five color-singlet channels are all higher than the corresponding thresholds, indicating that none of them forms a bound state. In addition, the energies of both color-exotic channels are above that of the lowest color-singlet ($J/\psi J/\psi$) channel. When only the coupling of the three S-wave channels is considered, the energy $E_{\rm mix1}$ is 6201 MeV, which is higher than the lowest $J/\psi J/\psi$ threshold. After four channels ($\chi_{c0}\chi_{c2}$, $\chi_{c1}\chi_{c1}$, $\chi_{c1}\chi_{c2}$, $\chi_{c2}\chi_{c2}$) composed of excited mesons are added and all seven channels are coupled, the lowest energy $E_{\rm mix2}$ remains almost unchanged. This indicates that, after channel coupling, the newly added channels do not substantially contribute to forming a bound state below the lowest threshold. This is mainly due to the large mass gap between these four channels and the three S-wave channels. In addition, the numerical results for the contributions of each term in the Hamiltonian are shown in Table 5. As shown in Table 5,

Table 4. Results of bound-state calculations for the $c\bar{c}c\bar{c}$ system with $J^{PC} = 2^{++}$ (in MeV).

Channel	$\|[LS]_i F_j C_k\rangle$	$E_{\rm th}$	$E_{\rm sc}$	$E_{\rm mix1}$	$E_{\rm mix2}$
$J/\psi J/\psi$	$\|211\rangle$	6200	6201	6201	6201
$\chi_{c0}\chi_{c2}$	$\|111\rangle$	6943	6946		
$\chi_{c1}\chi_{c1}$	$\|311\rangle$	6958	6960		
$\chi_{c1}\chi_{c2}$	$\|511\rangle$	7002	7005		
$\chi_{c2}\chi_{c2}$	$\|412\rangle$	7046	7050		
$[J/\psi]_8[J/\psi]_8$	$\|212\rangle$		6437		
$[cc]^1_{\bar{3}}[\bar{c}\bar{c}]^1_3$	$\|223\rangle$		6485		

Table 5. Numerical results for the contributions of each term in the Hamiltonian with $J^{PC}=2^{++}$ in the $cc\bar{c}\bar{c}$ system (unit: MeV).

Channel	$J/\psi J/\psi$	$\chi_{c0}\chi_{c2}$	$\chi_{c1}\chi_{c1}$	$\chi_{c1}\chi_{c2}$	$\chi_{c2}\chi_{c2}$	$[J/\psi]_8[J/\psi]_8$	$[cc]^1_3[\bar{c}\bar{c}]^1_{\bar{3}}$	$E_{\rm mix1}$	$E_{\rm mix2}$
mass	6600	6600	6600	6600	6600	6600	6600	6600	6600
E_k	682	777	754	709	664	630	670	682	682
$V^{\rm C}_{\rm CON}$	−15	227	230	255	280	56	62	−15	−15
$V^{\rm SO}_{\rm CON}$	0	1	1	0	−2	0	0	0	0
$V^{\rm C}_{\rm OGE}$	−1066	−586	−579	−559	−538	−849	−847	−1066	−1066
$V^{\rm SO}_{\rm OGE}$	0	−52	−61	−6	49	0	0	0	0
$V^{\rm T}_{\rm OGE}$	0	−21	15	6	−3	0	0	0	0
total	6201	6946	6960	7005	7050	6437	6485	6201	6201

the spin-orbit coupling effect appears only in channels composed of excited mesons. This is because, for channels formed by ground-state mesons, the orbital angular momentum is $L=0$, so the spin-orbit coupling does not contribute. For channels composed of excited mesons, except for the $V^{\rm SO}_{\rm OGE}$ term in the $\chi_{c0}\chi_{c0}$ channel, which is repulsive, the other channels provide attractive potentials. The $V^{\rm C}_{\rm OGE}$ term in all channels provides most of the attractive potential, but it is not sufficient to lower the energy below the corresponding thresholds. After channel coupling, because no bound state is formed, the respective contributions of each term to $E_{\rm mix1}$ and $E_{\rm mix2}$ are essentially identical to those in the individual $J/\psi J/\psi$ channel. Therefore, there is no bound state below the lowest threshold (6200 MeV) in this system.

For color-excited structures, color confinement prevents direct dissociation. Therefore, these structures may form resonant states. To identify genuine resonant states in this system, the real-scaling method is employed, and the corresponding results are presented in Figs. 2 and 3. It should be noted that, when a large number of channels are coupled, avoided-crossing structures can also form because the scattering channels descend to the threshold line at different rates. Thus, it is necessary to calculate the components of the resonant state to determine whether it is a genuine resonant state.

In Fig. 2, the thresholds of $J/\psi J/\psi$ and $J/\psi\psi(2S)$ are indicated by red horizontal lines. Near the energies of 7002 and 7223 MeV, two avoided-crossing structures are marked by red circles and denoted as $R(7002)$ and $R(7223)$, respectively. In addition, the color-structure proportions of $R(7002)$ and $R(7223)$ are 90% (45% from the $\bar{3}\otimes 3$ configuration) and 92% (71% from the $\bar{3}\otimes 3$ configuration), respectively. Therefore, we regard these two structures as genuine resonance states. To calculate the decay widths of the resonance states, we employ Eq. (18), as described in Section III. The decay widths obtained for $R(7002)$ and $R(7223)$ are 54 and 66 MeV, respectively.

Figure 3 shows that the red horizontal lines, from bottom to top, represent the thresholds of $J/\psi J/\psi$, $J/\psi\psi(2S)$,

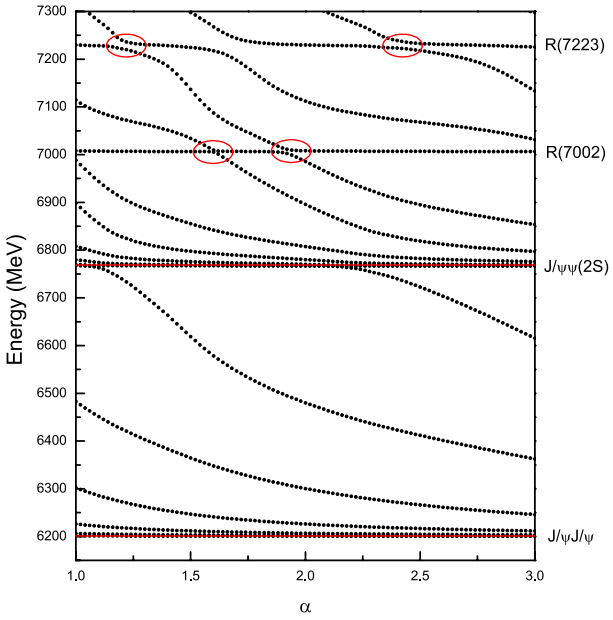


Fig. 2. (color online) Stabilization plots of the energies obtained by including three channels ($J/\psi J/\psi$, $[J/\psi]_8[J/\psi]_8$, $[cc]^1_3[\bar{c}\bar{c}]^1_{\bar{3}}$) in the $cc\bar{c}\bar{c}$ system with $J^{PC}=2^{++}$.

$\chi_{c0}\chi_{c2}$, $\chi_{c1}\chi_{c1}$, $\chi_{c1}\chi_{c2}$, $\chi_{c2}\chi_{c2}$, and $J/\psi\psi(3S)$, respectively. At an energy of approximately 7227 MeV, three avoided-crossing structures are marked by red circles. This suggests the possible presence of a resonant state near this energy, denoted as $R(7227)$. The calculation shows that the component at 7227 MeV is dominated by color configurations, accounting for 82% (51% from the $\bar{3}\otimes 3$ configuration). Therefore, the resonant state $R(7227)$ is a genuine resonant state rather than a spurious resonance formed by scattering states. Furthermore, the decay width obtained for $R(7227)$ is 61 MeV.

In Fig. 3, the energy levels near 6980 – 7080 MeV are too dense to directly determine the presence of a resonant state. To more clearly reveal the avoided-crossing structures in this region, we enlarge this energy range, as shown in Fig. 4. Figure 4 clearly shows two avoided-crossing structures (marked by red circles) near the en-

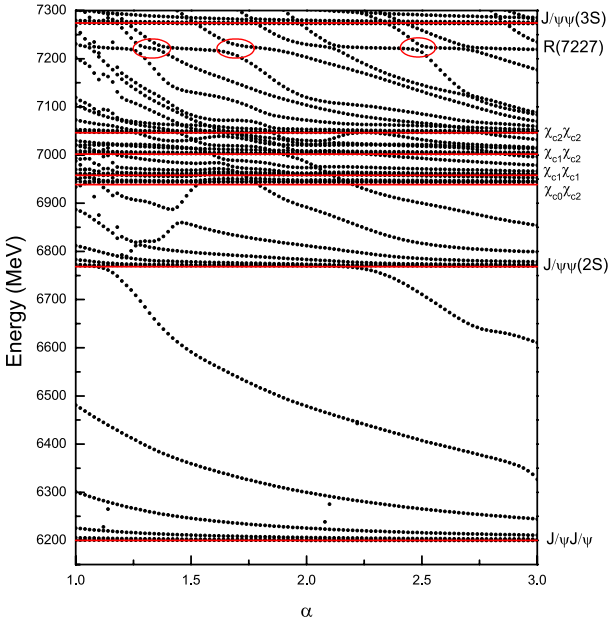


Fig. 3. (color online) Stabilization plots for the energies obtained by including seven channels in the $cc\bar{c}\bar{c}$ system with $J^{PC} = 2^{++}$.

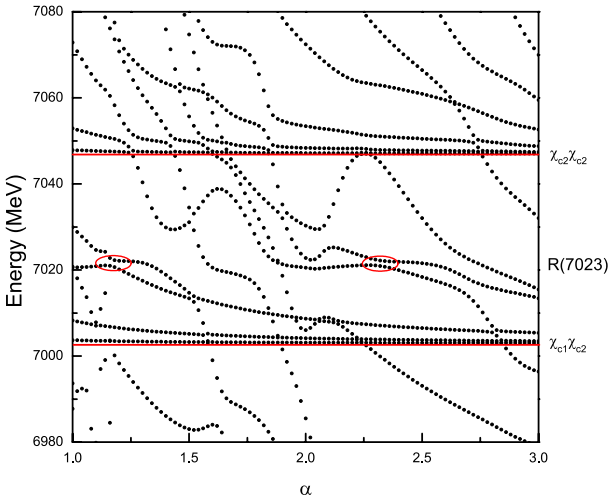


Fig. 4. (color online) Stabilization plots of the energies obtained by including seven channels in the $cc\bar{c}\bar{c}$ system with $J^{PC} = 2^{++}$ (energy range: 6980–7080 MeV).

ergy of 7023 MeV, denoted as $R(7023)$. Moreover, the dominant component of $R(7023)$ is color configurations, accounting for 65% (42% from the $\bar{3}\otimes 3$ configuration). Therefore, it is a genuine resonant state. From Eq. (18), its width is calculated to be 43 MeV.

The above results indicate that the two resonances $R(7223)$ and $R(7002)$ in Fig. 3 persist after the inclusion of channels consisting of excited mesons, but their energies are shifted upward because of the interaction between the new channels and the original resonances. Therefore, we conclude that $R(7223)$ and $R(7227)$ correspond to the same resonance, and similarly that $R(7002)$ and $R(7023)$ correspond to the same resonance. We retain the former designation for each, namely $R(7223)$ and $R(7002)$. The resonant state $R(7002)$ may serve as a candidate for the $X(6900)$, while $R(7223)$ is a good candidate for the $X(7200)$. In addition, from the perspective of their structural proportions, the resonance $R(7002)$ tends to have a molecular structure, whereas $R(7223)$ is more likely to have a compact tetraquark structure. In Ref. [38], the authors suggest that, for the $cc\bar{c}\bar{c}$ system with $J^{PC} = 2^{++}$, the lower resonant state with mass $M \approx 7000$ MeV and width $\Gamma \approx 75$ MeV may serve as a candidate for the $X(6900)$. Meanwhile, a higher resonant state with mass $M \approx 7200$ MeV and width $\Gamma \approx 50$ MeV could be a candidate for the $X(7200)$. This is consistent with the conclusion obtained here.

B. Fully bottomed tetraquark system

The energies of the $bb\bar{b}\bar{b}$ tetraquark system with $J^{PC} = 2^{++}$ are presented in Table 6. The numerical results in Table 6 show that, for the $b\bar{b}$-$b\bar{b}$ structures, no bound state lies below the corresponding thresholds. In addition, the energy of bb-$\bar{b}\bar{b}$ is several hundred MeV higher than the lowest threshold (18998 MeV). In the channel-coupling calculations, no bound state is found below the lowest threshold, regardless of whether channels composed of excited mesons ($\chi_{b0}\chi_{b2}$, $\chi_{b1}\chi_{b1}$, $\chi_{b1}\chi_{b2}$, $\chi_{b2}\chi_{b2}$) are included. The numerical results for the contributions from each term in the Hamiltonian are shown in Table 7. Similar to the cccc system, the $V^{\rm C}_{\rm OGE}$ term provides most of the attractive potential, but it is insufficient to produce a bound state.

Furthermore, the real-scaling method is also used to search for genuine resonance states in this system. The results are shown in Figs. 5 and 6. In Fig. 5, the red horizontal lines from bottom to top represent the thresholds of $\Upsilon\Upsilon$, $\Upsilon\Upsilon(2S)$, and $\Upsilon\Upsilon(3S)$, respectively. Near the energy of 19743 MeV, the avoided-crossing structures are marked by red circles and denoted as $R(19743)$. Moreover, the color-structure proportion at the energy of 19743 MeV is 88% (66% from the $\bar{3}\otimes 3$ configuration). Therefore, the state $R(19743)$ is a genuine resonance

Table 6. Results of the bound-state calculations for the $b\bar{b}b\bar{b}$ system with $J^{PC} = 2^{++}$ (in MeV).

Channel	$\|[LS]_i F_j C_k\rangle$	$E_{\rm th}$	$E_{\rm sc}$	$E_{\rm mix1}$	$E_{\rm mix2}$
$\Upsilon\Upsilon$	$\|211\rangle$	19904	19005	19005	19005
$\chi_{b0}\chi_{b2}$	$\|111\rangle$	19773	19774		
$\chi_{b1}\chi_{b1}$	$\|311\rangle$	19782	19782		
$\chi_{b1}\chi_{b2}$	$\|511\rangle$	19799	19801		
$\chi_{b2}\chi_{b2}$	$\|412\rangle$	19816	19818		
$[\Upsilon]_8[\Upsilon]_8$	$\|212\rangle$		19284		
$[bb]^1_{\bar{3}}[\bar{b}\bar{b}]^1_3$	$\|223\rangle$		19330		

Table 7. Numerical results for the contributions of each term in the Hamiltonian with $J^{PC}=2^{++}$ in the $bb\bar{b}\bar{b}$ system (units: MeV).

Channel	$\Upsilon\Upsilon$	$\chi_{b0}\chi_{b2}$	$\chi_{b1}\chi_{b1}$	$\chi_{b1}\chi_{b2}$	$\chi_{b2}\chi_{b2}$	$[\Upsilon]_8[\Upsilon]_8$	$[bb]^1_3[\bar{b}\bar{b}]^1_3$	$E_{\rm mix1}$	$E_{\rm mix2}$
mass	19908	19908	19908	19908	19908	19908	19908	19908	19908
E_k	803	563	545	520	494	651	642	803	803
$V^{\rm C}_{\rm CON}$	−138	2	4	12	20	−111	−100	−138	−138
$V^{\rm SO}_{\rm CON}$	0	≈0	0.1	0	−0.1	0	0	0	0
$V^{\rm C}_{\rm OGE}$	−1568	−668	−658	−640	−623	−1164	−1120	−1568	−1568
$V^{\rm SO}_{\rm OGE}$	0	−21	−24	−2	20	0	0	0	0
$V^{\rm T}_{\rm OGE}$	0	−10	7	3	−1	0	0	0	0
total	19005	19774	19782	19801	19818	19284	19330	19005	19005

state. The decay width of $R(19743)$ is obtained as 68 MeV. In addition, avoided-crossing structures also form at an energy around 19645 MeV. However, their composition is dominated by scattering channels, which account for 64%. Therefore, we conclude that this type of avoided-crossing structure is caused by the different rates at which the scattering channels descend to the threshold line. Accordingly, it is a false resonant state at an energy around 19645 MeV.

In Fig. 6, the red horizontal lines from bottom to top represent the thresholds of $\Upsilon\Upsilon$, $\Upsilon\Upsilon(2S)$, $\chi_{b0}\chi_{b2}$, $\chi_{b1}\chi_{b1}$, $\Upsilon\Upsilon(3S)$, $\chi_{b1}\chi_{b2}$, and $\chi_{b2}\chi_{b2}$, respectively. At the energy of 19745 MeV, two avoided-crossing structures are marked by red circles. A resonant state may exist here, and it is denoted as $R(19745)$. The 79% color-structure proportion (64% from the $\bar{3}\otimes 3$ configuration) indicates that

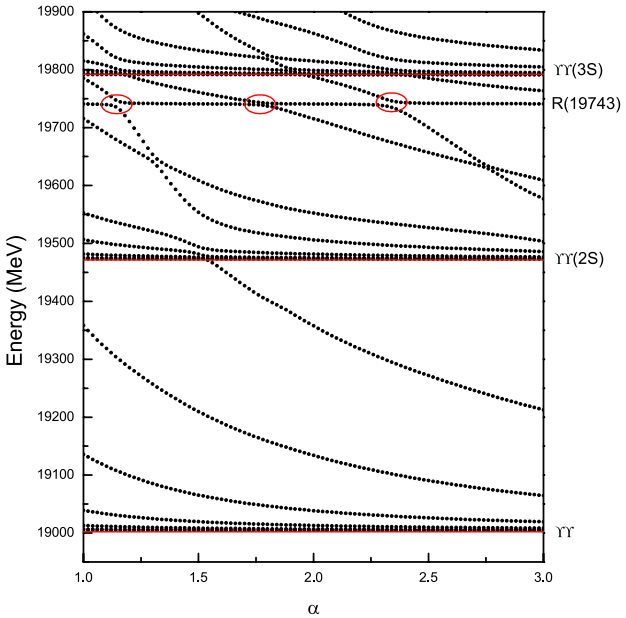


Fig. 5. (color online) Stabilization plots of the energies for the three channels ($\Upsilon\Upsilon$, $[\Upsilon]_8[\Upsilon]_8$, and $[bb]^1_3[\bar{b}\bar{b}]^1_3$) in the $bb\bar{b}\bar{b}$ system with $J^{PC}=2^{++}$.

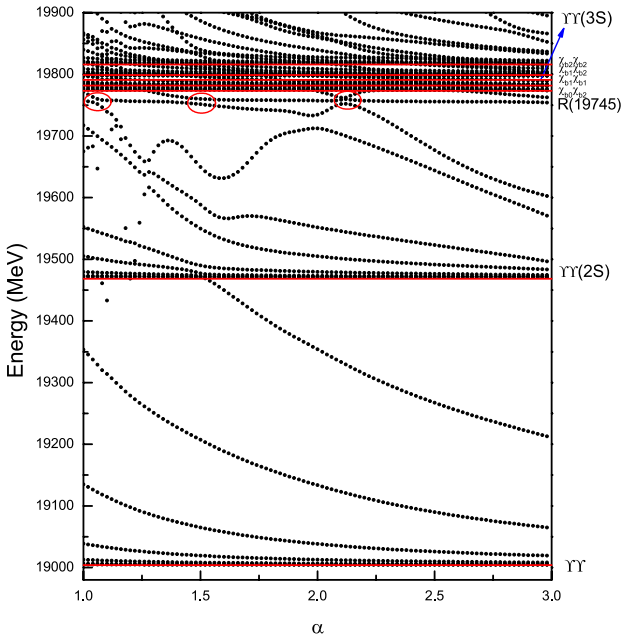


Fig. 6. (color online) Stabilization plots of the energies for the seven-channel calculation in the $bb\bar{b}\bar{b}$ system with $J^{PC}=2^{++}$.

$R(19745)$ is a genuine resonant state, and its decay width is 64 MeV. The newly added channels $\chi_{b0}\chi_{b2}$, $\chi_{b1}\chi_{b1}$, $\chi_{b1}\chi_{b2}$, and $\chi_{b2}\chi_{b2}$ do not cause $R(19743)$ in Fig. 5 to vanish, because the energies of these channels are all above that of $R(19743)$. Thus, it cannot decay through these channels. In addition, from the perspective of their structural proportions, the resonance $R(19743)$ is more likely to have a compact tetraquark structure.

Using the same procedure as that for the $cc\bar{c}\bar{c}$ system, we performed a detailed examination of the energy region from 19770 to 19860 MeV in Fig. 6 (as shown in Fig. 7). The results show that the avoided-crossing structures are dominated by threshold-channel configurations, and hence no resonance states exist.

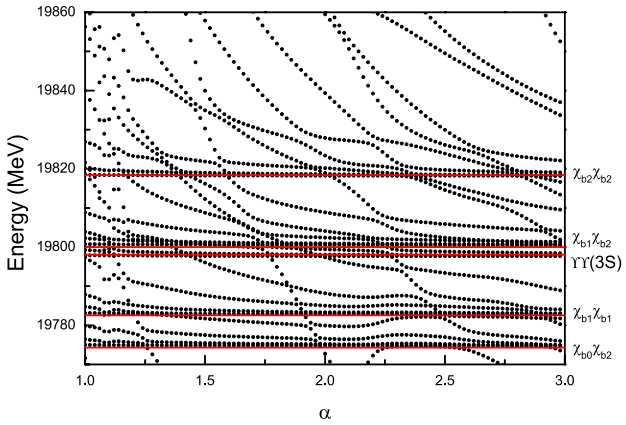


Fig. 7. (color online) Stabilization plots for the energies of seven channels in the $bb\bar{b}\bar{b}$ system with $J^{PC}=2^{++}$ (energy range: 19770–19860).

V. SUMMARY

In this work, we systematically investigate fully charmed and fully bottomed tetraquark systems with $J^{PC}=2^{++}$ in the framework of the ChQM. Two structures, $Q\bar{Q}-Q\bar{Q}$ and $QQ-\bar{Q}\bar{Q}$, as well as the coupling between these two configurations, are considered. A dynamical bound-state calculation is performed to search for bound states in the fully heavy systems. In addition, a stabilization calculation (real-scaling method) is performed to identify resonance states.

The bound-state calculation shows that no bound state lies below the lowest threshold for the $cc\bar{c}\bar{c}$ and $bb\bar{b}\bar{b}$ systems with $J^{PC}=2^{++}$. However, in the $cc\bar{c}\bar{c}$ system, two resonant states, $R(7002)$ and $R(7227)$, are obtained using the real-scaling method. The decay widths of these two resonant states are 54 MeV and 66 MeV, respectively. $R(7002)$ can be regarded as a candidate for the $X(6900)$, while $R(7227)$ corresponds to $X(7200)$. Our results are consistent with Ref. [38] for the $J^{PC}=2^{++}$ system, in which the resonant state with mass $M\approx 7000$ MeV and width $\Gamma\approx 75$ MeV may serve as a candidate for the $X(6900)$. In addition, a higher resonant state with mass $M\approx 7200$ MeV and width $\Gamma\approx 50$ MeV could be a candidate for the $X(7200)$.

In the $bb\bar{b}\bar{b}$ system, one resonant state is obtained at an energy of around 19743 MeV. The decay width of this resonant state is around 68 MeV. Moreover, in Ref. [38], the authors also obtained a resonant state with a mass of 19788 MeV and a width of 60 MeV. We propose experimentally searching for these possible resonant states with a larger data sample in the invariant mass spectrum of ϒϒ or ϒϒ$(2S)$.

References

[1] S. K. Choi *et al*. (Belle Collaboration), Phys. Rev. Lett. **91**, 262001 (2003)
[2] V. Khachatryan *et al*. (CMS Collaboration), JHEP **05**, 013 (2017)
[3] L. C. Bland *et al.* (ANDY Collaboration), arXiv: 1909.03124[nucl-ex]
[4] R. Aaij *et al*. (LHCb Collaboration), JHEP **10**, 086 (2018)
[5] A. M. Sirunyan *et al*. (CMS Collaboration), Phys. Lett. B **808**, 135578 (2020)
[6] W. Chen, H. X. Chen, X. Liu *et al*., Phys. Lett. B **773**, 247 (2017)
[7] Y. Bai, S. Lu and J. Osborne, Phys. Lett. B **798**, 134930 (2019)
[8] Q. N. Wang, Z. Y. Yang and W. Chen, Phys. Rev. D **104**, 114037 (2021)
[9] C. Hughes, E. Eichten, and C. T. H. Davies, Phys. Rev. D **97**, 054505 (2018)
[10] E. Eichten and Z. Liu, arXiv: 1709.09605[hep-ph]
[11] R. Aaij *et al*. (LHCb Collaboration), Sci. Bull. **65**, 1983 (2020)
[12] A. Hayrapetyan *et al*. (CMS Collaboration), Phys. Rev. Lett. **132**, 111901 (2024)
[13] G. Aad *et al*. (ATLAS Collaboration), Phys. Rev. Lett. **131**, 151902 (2023)
[14] Y. Iwasaki, Prog. Theor. Phys. **54**, 492 (1975)
[15] Y. Iwasaki, Phys. Rev. Lett. **36**, 1266 (1976)
[16] K. T. Chao, Z. Phys. C **7**, 317 (1981)
[17] J. P. Ader, J. M. Richard, and P. Taxil, Phys. Rev. D **25**, 2370 (1982)
[18] L. Heller and J. A. Tjon, Phys. Rev. D **32**, 755 (1985)
[19] R. J. Lloyd and J. P. Vary, Phys. Rev. D **70**, 014009 (2004)
[20] N. Barnea, J. Vijande, and A. Valcarce, Phys. Rev. D **73**, 054004 (2006)
[21] J. Vijande, A. Valcarce, and N. Barnea, Phys. Rev. D **79**, 074010 (2009)
[22] A. V. Berezhnoy, A. V. Luchinsky, and A. A. Novoselov, Phys. Rev. D **86**, 034004 (2012)
[23] Z. G. Wang, Eur. Phys. J. C **77**, 432 (2017)
[24] M. Karliner, S. Nussinov, and J. L. Rosner, Phys. Rev. D **95**, 034011 (2017)
[25] M. N. Anwar, J. Ferretti, F. K. Guo *et al*., Eur. Phys. J. C **78**, 647 (2018)
[26] J. Wu, Y. R. Liu, K. Chen *et al*., Phys. Rev. D **97**, 094015 (2018)
[27] W. Chen, H. X. Chen, X. Liu *et al*., EPJ Web Conf. **182**, 02028 (2018)
[28] V. R. Debastiani and F. S. Navarra, Chin. Phys. C **43**, 013105 (2019)
[29] G. J. Wang, L. Meng, and S. L. Zhu, Phys. Rev. D **100**, 096013 (2019)
[30] J. M. Richard, A. Valcarce, and J. Vijande, Phys. Rev. D **95**, 054019 (2017)
[31] M. S. Liu, Q. F. Lü, X. H. Zhong *et al*., Phys. Rev. D **100**, 016006 (2019)
[32] Z. G. Wang and Z. Y. Di, Acta Phys. Polon. B **50**, 1335 (2019)
[33] M. A. Bedolla, J. Ferretti, C. D. Roberts *et al*., Eur. Phys. J. C **80**, 1004 (2020)
[34] C. Deng, H. Chen, and J. Ping, Phys. Rev. D **103**, 014001

(2021)
[35] X. Jin, Y. Xue, H. Huang *et al.*, Eur. Phys. J. C **80**, 1083 (2020)
[36] Q. F. Lü, D. Y. Chen, and Y. B. Dong, Eur. Phys. J. C **80**, 871 (2020)
[37] J. Zhang, J. B. Wang, G. Li *et al.*, Eur. Phys. J. C **82**, 1126 (2022)
[38] W. L. Wu, Y. K. Chen, L. Meng *et al.*, Phys. Rev. D **109**, 054034 (2024)
[39] J. F. Giron and R. F. Lebed, Phys. Rev. D **102**, 074003 (2020)
[40] G. Yang, J. Ping and J. Segovia, Phys. Rev. D **104**, 014006 (2021)
[41] W. L. Wu and S. L. Zhu, Phys. Rev. D **111**, 034044 (2025)
[42] D. D. Lu and S. Z. Jiang, Phys. Rev. D **113**, 094034 (2026)
[43] M. S. liu, F. X. Liu, X. H. Zhong *et al.*, Phys. Rev. D **109**, 076017 (2024)
[44] Z. Zhao, K. Xu, A. Kaewsnod *et al.*, Phys. Rev. D **103**, 116027 (2021)
[45] G. J. Wang, L. Meng, M. Oka *et al.*, Phys. Rev. D **104**, 036016 (2021)
[46] F. X. Liu, M. S. Liu, X. H. Zhong *et al.*, Phys. Rev. D **104**, 116029 (2021)
[47] Z. G. Wang, Chin. Phys. C **44**, 113106 (2020)
[48] C. M. Tang, C. G. Duan, and L. Tang, Eur. Phys. J. C **84**, 743 (2024)
[49] B. C. Yang, L. Tang, and C. F. Qiao, Eur. Phys. J. C **81**, 324 (2021)
[50] S. S. Agaev, K. Azizi, B. Barsbay *et al.*, Phys. Lett. B **844**, 138089 (2023)
[51] S. S. Agaev, K. Azizi, B. Barsbay *et al.*, Eur. Phys. J. C **83**, 994 (2023)
[52] S. S. Agaev, K. Azizi, B. Barsbay *et al.*, Nucl. Phys. A **1041**, 122768 (2024)
[53] G. L. Yu, Z. Y. Li, Z. G. Wang *et al.*, Eur. Phys. J. C **83**, 416 (2023)
[54] W. C. Dong and Z. G. Wang, Phys. Rev. D **107**, 074010 (2023)
[55] R. H. Wu, Y. S. Zuo, C. Y. Wang *et al.*, JHEP **11**, 023 (2022)
[56] Z. Z. Chen, X. L. Chen, P. F. Yang *et al.*, Phys. Rev. D **109**, 094011 (2024)
[57] Z. G. Wang, Int. J. Mod. Phys. A **36**, 2150014 (2021)
[58] B. D. Wan and C. F. Qiao, Phys. Lett. B **817**, 136339 (2021)
[59] Z. G. Wang, Nucl. Phys. B **985**, 115983 (2022)
[60] H. Mutuk, Eur. Phys. J. C **81**, 367 (2021)
[61] Y. Y. Lin, J. Y. Wang, and A. Zhang, Eur. Phys. J. Plus **139**, 707 (2024)
[62] Q. Huang, R. Chen, J. He *et al.*, Phys. Rev. D **113**, 074007 (2026)
[63] J. Zhao, S. Shi, and P. Zhuang, Phys. Rev. D **102**, 114001 (2020)
[64] H. W. Ke, X. Han, X. H. Liu *et al.*, Eur. Phys. J. C **81**, 427 (2021)
[65] Q. Li, C. H. Chang, G. L. Wang *et al.*, Phys. Rev. D **104**, 014018 (2021)
[66] M. Karliner and J. L. Rosner, Phys. Rev. D **102**, 114039 (2020)
[67] R. M. Albuquerque, S. Narison, A. Rabemananjara *et al.*, Phys. Rev. D **102**, 094001 (2020)
[68] M. C. Gordillo, F. De Soto, and J. Segovia, Phys. Rev. D **102**, 114007 (2020)
[69] Z. R. Liang, X. Y. Wu, and D. L. Yao, Phys. Rev. D **104**, 034034 (2021)
[70] S. Pal, R. Ghosh, B. Chakrabarti *et al.*, Eur. Phys. J. Plus **136**, 625 (2021)
[71] P. G. Ortega, D. R. Entem, and F. Fernández, Phys. Rev. D **108**, 094023 (2023)
[72] R. Zhu, Nucl. Phys. B **966**, 115393 (2021)
[73] F. G. Celiberto, Phys. Rev. D **112**, 074041 (2025)
[74] Y. Wang, R. Li, and B. Zhong *et al.*, arXiv: 2604.18061[hep-ex]
[75] H. B. Liang, W. B. Li, and W. N. Liu, Eur. Phys. J. Plus **141**, 358 (2026)
[76] X. Liu, Y. Wang, and R. Zhu, arXiv: 2512.22070[hep-ph]
[77] J. Z. Wang, D. Y. Chen, X. Liu *et al.*, Phys. Rev. D **103**, 071503 (2021)
[78] K. T. Chao and S. L. Zhu, Sci. Bull. **65**, 1952 (2020)
[79] X. K. Dong, V. Baru, F. K. Guo *et al.*, Phys. Rev. Lett. **126**, 132001 (2021) [Erratum: Phys. Rev. Lett. **127**, 119901 (2021)]
[80] H. F. Zhang, Y. Q. Ma, and W. L. Sang, Sci. Bull. **70**, 1915 (2025)
[81] Z. H. Guo and J. A. Oller, Phys. Rev. D **103**, 034024 (2021)
[82] Q. F. Cao, H. Chen, H. R. Qi *et al.*, Chin. Phys. C **45**, 103102 (2021)
[83] Q. Zhou, D. Guo, S. Q. Kuang *et al.*, Phys. Rev. D **106**, L111502 (2022)
[84] Z. G. Wang and X. S. Yang, AAPPS Bull. **34**, 5 (2024)
[85] S. S. Agaev, K. Azizi, B. Barsbay *et al.*, Eur. Phys. J. Plus **138**, 935 (2023)
[86] G. Li, X. F. Wang, and Y. Xing, Eur. Phys. J. C **79**, 645 (2019)
[87] H. X. Chen, W. Chen, X. Liu *et al.*, Sci. Bull. **65**, 1994 (2020)
[88] C. Becchi, J. Ferretti, A. Giachino *et al.*, Phys. Lett. B **811**, 135952 (2020)
[89] K. Chen, F. X. Liu, Q. Zhao *et al.*, arXiv: 2412.13455 [hep-ph]
[90] X. S. Yang and Z. G. Wang, arXiv: 2409.05428[hep-ph]
[91] F. Feng and M. M. Liu, Phys. Rev. D **113**, 054010 (2026)
[92] X. Y. Wang, Q. Y. Lin, H. Xu *et al.*, Phys. Rev. D **102**, 116014 (2020)
[93] H. H. Ma, Z. K. Tao, and J. J. Niu, arXiv: 2502.20891 [hep-ph]
[94] X. W. Bai, Y. Huang, and W. L. Sang, Phys. Rev. D **111**, 054006 (2025)
[95] X. W. Bai, F. Feng, C. M. Gan *et al.*, JHEP **09**, 002 (2024)
[96] F. Feng, Y. Huang, Y. Jia *et al.*, Phys. Rev. D **110**, 054007 (2024)
[97] R. Maciuła, W. Schäfer, and A. Szczurek, Phys. Lett. B **812**, 136010 (2021)
[98] V. P. Gonçalves and B. D. Moreira, Phys. Lett. B **816**, 136249 (2021)
[99] F. Feng, Y. Huang, Y. Jia *et al.*, Phys. Rev. D **108**, L051501 (2023)
[100] Y. Wang and R. Zhu, arXiv: 2510.02085[hep-ph]
[101] F. G. Celiberto, A. V. Giannini, V. P. Gonçalves *et al.*, Phys. Rev. D **113**, 054014 (2026)
[102] F. Feng, Y. Huang, Y. Jia *et al.*, Phys. Rev. D **106**, 114029 (2022)
[103] C. Gong, M. C. Du, Q. Zhao *et al.*, Phys. Lett. B **824**, 136794 (2022)
[104] Y. Wu, X. Liu, J. Ping *et al.*, Eur. Phys. J. C **85**, 147

(2025)
[105] A. Hayrapetyan *et al*. (CMS Collaboration), Nature **648**, 8092 (2025)
[106] J. Vijande, F. Fernandez, and A. Valcarce, J. Phys. G **31**, 481 (2005)
[107] S. Navas *et al*. (Particle Data Group), Phys. Rev. D **110**, 030001 (2024)
[108] E. Hiyama, Y. Kino, and M. Kamimura, Prog. Part. Nucl. Phys. **51**, 223 (2003)
[109] J. Simons, J. Chem. Phys. **75**, 2465 (1981)
[110] Y. Tan and J. Ping, Chin. Phys. C **45**, 093104 (2021)
[111] E. Hiyama, M. Kamimura, A. Hosaka *et al*., Phys. Lett. B **633**, 237 (2006)
[112] E. Hiyama, A. Hosaka, M. Oka *et al*., Phys. Rev. C **98**, 045208 (2018)
[113] H. Huang, C. Deng, X. Liu *et al*., Symmetry **15**, 1298 (2023)
[114] Y. Wu, X. Jin, R. Liu *et al*., Phys. Rev. D **107**, 094011 (2023)
[115] Y. Wu, Y. Yan, Y. Tan *et al*., Phys. Rev. D **109**, 096005 (2024)